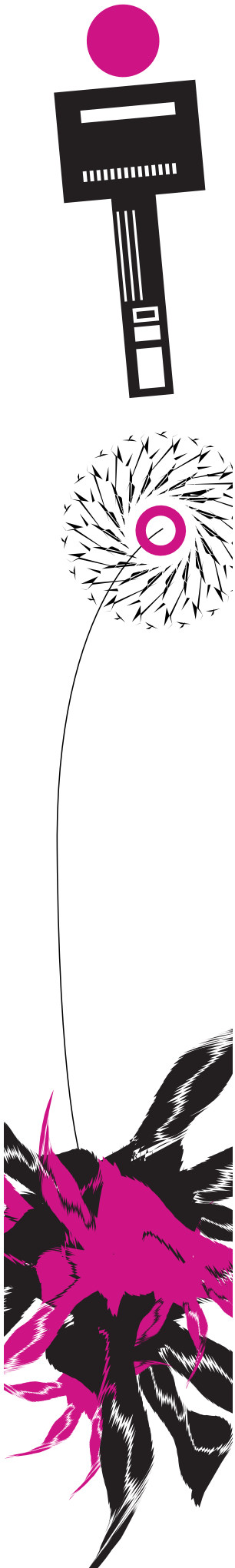

RAM ROBOTICS AND MECHATRONICS

# CONTROL OF REDUNDANT MECHANICAL SYSTEMS IN THE PRESENCE OF EXTERNAL DISTURBANCES

A. (Ahmed) Tamer Salah Abdo Ali

BSC ASSIGNMENT

**Committee:**
prof. dr. ir. A. Franchi
C. Gabellieri, Ph.D
dr. ir. G. Meinsma

July, 2022

030RaM2022
Robotics and Mechatronics
EEMCS
University of Twente
P.O. Box 217
7500 AE Enschede
The Netherlands

UNIVERSITY OF TWENTE. | TECHMED CENTRE
UNIVERSITY OF TWENTE. | DIGITAL SOCIETY INSTITUTE

# CONTROL OF REDUNDANT MECHANICAL SYSTEMS IN THE PRESENCE OF EXTERNAL DISTURBANCES

Ahmed Tamer
2206161

***Abstract*—Among the aerial robots, one class is an unmanned aerial manipulator consisting of a rotorcraft unmanned aerial vehicle and a redundant multi-link robotic arm. It makes it possible to carry out manipulation tasks with a flying robot. Stable and efficient position control can be crucial for carrying out manipulation tasks with an aerial manipulator. This paper focuses on exploiting redundancy in the presence of wind gusts while approaching the desired position steadily. Redundancy is exploited by executing numerical experiments of varying parameters while adding disturbances. An output linear quadratic regulator controller algorithm was created and implemented explicitly for controlling the aerial manipulator performing tasks in environments with wind disturbances. Results from the simulated linearized aerial manipulator model on Simulink® demonstrate how and which parameter changes affect the performance—measured by the maximum deviation of the controlled position, convergence time, and control effort. Simulation outputs also present that the designed controller can effectively reject the wind disturbance with proper parameter tuning. Finally, redundancy in this model has shown to have better accuracy in maintaining the referenced position.**

## I. Introduction

The field of aerial robots that physically interact with the environment, and in particular the unmanned aerial vehicles (UAVs) equipped with a manipulator, has been daily growing during the last 10 years [8]. The unmanned aerial manipulators (UAMs) field, is a popular research topic not only because of its challenges in perception and control, but also because of its promising potential for various industrial applications, including construction, transportation of goods, and mainly manipulation in dangerous places challenging to be reached by humans. For instance, the task of cleaning Burj Khalifa skyscraper is illustrated in Fig. 1, which shows that it is a very challenging, high-risk task for even professional climbers. Also, it is worth mentioning that the very high cost of such a job by humans. However, an aerial vehicle that is able to carry out simple manipulation tasks could help humanity in such kinds of activities as shown in Fig. 1 an example of a window cleaning UAV.

Keeping in mind the mentioned desired tasks for aerial manipulators, from a general point of view, it can be seen that UAVs have to be equipped with manipulation skills like grasping, assembly of mechanical parts, accurate positioning, transporting, etc. Many empirical studies propose multiple different solutions for UAV manipulation. For example, equipping the UAV with one or multiple manipulators like robotic arms or mounting a fixed gripper, or a rigid tool, or a cable directly on the UAV. As for this research paper, the former method will be discussed more as it is within the scope of this letter's purpose. Therefore, a UAM could be an efficient solution providing an aerial vehicle with the capability of performing dexterous manipulation tasks [8].

The goal is to design and simulate a controller for the aerial vehicle to perform accurate tracking of its end-effector. The whole idea can be pictured by a hummingbird reaching with its long beak for extracting nectar from a flower while keeping its body hovering in a stable manner in the air, as illustrated in Fig. 2. Nowadays, there are different researches about Bio-inspired UAVs, but this is not the focus of this paper. The focus is controlling a multirotor UAM, which can be pictured to behave like the hummingbird in Fig. 2, manipulating an end-effector while stably hovering in the air compensating for external disturbances.

Controlling such a task is considered challenging for the following reasons; external disturbances like wind gusts are not perfectly known [14], actuators may introduce some mechanical limits, and understanding if redundancy can be utilized to improve the performance of the system while achieving the control objectives. Within the context of this paper, redundancy means the number of control inputs is greater than the dimension of the task.

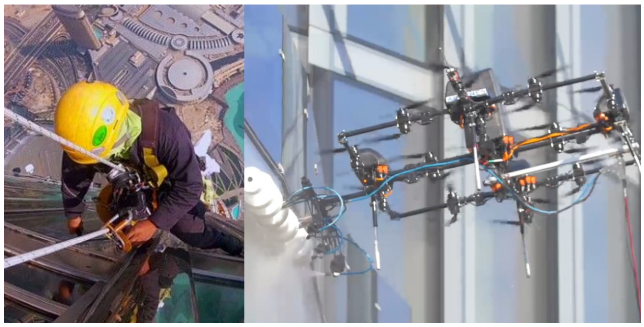

Fig. 1: A typical scenario where a worker is cleaning windows at a skyscraper (Left) URL as compared to an aerial robotic worker performs the same task (Right) URL.

Fig. 2: Humming Birds manipulating their beaks to extract nectar URL.

## II. System Modelling

Considering an unmanned aerial vehicle equipped with a mounted end-effector tool, a 1-DoF manipulator moving in lateral dynamics can be modelled as a planar model of a 2-DoF mass spring damper system, as illustrated in Fig.3

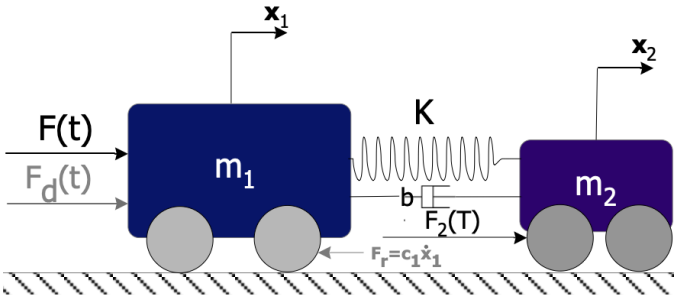


Fig. 3: Simplified dynamic model of a 2-Dof UAM with relevant parameters

Where $m_1$, $m_2$, $K$, $b$, $c_1$ represents the UAM body's mass, the end-effector's mass, spring stiffness constant, damping coefficient, and friction constant, respectively. Dynamic equations of the proposed system in Fig.3 were obtained using Newton's second law ($F_{net} = \frac{change\ in\ momentum}{change\ in\ time} = \frac{\Delta p}{\Delta t}$).

Equations of motion:

- $m_1\ddot{x}_1+\dot{x}_1(c_1+b)+Kx_1 = F(t)+F_d(t)+Kx_2+b\dot{x}_2$
- $m_2\ddot{x}_2 + b\dot{x}_2 + Kx_2 = F_2(t) + Kx_1 + b\dot{x}_1$

State space equations:

- $\dot{x} = Ax + Bu(t)$ and $y = Cx + Du(t)$
- $x = \begin{bmatrix} x_1 & x_2 & \dot{x}_1 & \dot{x}_2 \end{bmatrix}^T$
- $A = \begin{bmatrix} 0 & 0 & 1 & 0 \\ 0 & 0 & 0 & 1 \\ -\frac{K}{m_1} & \frac{K}{m_1} & -\frac{(c_1+b)}{m_1} & \frac{b}{m_1} \\ \frac{K}{m_2} & -\frac{K}{m_2} & \frac{b}{m_2} & -\frac{b}{m_2} \end{bmatrix}$
- $y = \begin{bmatrix} 0 & 1 & 0 & 0 \\ 0 & 0 & 0 & 1 \end{bmatrix} x$

According to the proposed model of a UAV, it is assumed to perform lateral motions only, i.e. translation along the $x-axis$. The main goal is to regulate the position of the second mass ($m_2$) while exploiting, if the second force input ($F_2(t)$) helps in achieving higher efficiency.

### A. Design Parameters

One of the early challenges faced was to find a set of well-tested parameters' values for the proposed dynamic model. In this paper, the Tilt-Hex robot, which is an LAAS-CNRS house developed fully actuated aerial robot was selected to be the reference for the required parameters' values. The reason for choosing Tilt-Hex was due to the fact that Franchi et al. [9] conducted extensive tests with different damping, stiffness, and mass values and being one of the few papers that provides clear and validated feedback on these conducted tests. The aerial manipulator system mainly consists of a hexrotor UAV, a variable-stiffness element end-effector. The main parameters of the modelled aerial manipulator are summarised in Table. I.

TABLE I: Parameters of modelled aerial manipulator

| Parameter | Value |
|---|---|
| **Tilt-Hex rotor mass** ($m_1$) | $1.86kg$ |
| **Manipulator mass** ($m_2$) | $0.54kg$ |
| **Manipulator's spring stiffness** ($K$) | $6kgs^{-2}$ |
| **Manipulator's damping coefficient** ($b$) | $10kgs^{-1}$ |
| **Friction constant** ($c_1$) | $1.0$ |
| **Arm length (spring natural length)** | $0.45m$ |

As for the applied input forces; $F(t)$ represents a maximum thrust of $60N$, which can be estimated from the propeller datasheet (MK3638 brushless motor from MikroKopter and 12" propellers). The listed maximum thrust is around $20N$, but a max thrust of $10N$ was selected instead to compensate for the total weight based on D. Bicego's et al. paper [3] on designing the Tilt-Hex rotor, and since there are six propellers, so the max thrust is assumed to be $60N$. $F_d(t)$ is considered a pulse in time domain with an amplitude of $1N$, so it contains a large spectrum of different frequencies in the frequency domain. $F_d(t)$ is only acting on the bigger mass ($m_1$), as it's size would be relatively large to the second mass ($m_2$). So, it is safe to assume that air resistance would impact mostly the bigger mass. Last but not least, $F_2(t)$ is representing the control input of the manipulator's (arm) joints. However, usually manipulators' joints are rotating by applying a certain torque. In this model, we have a linear problem hence it is represented by a linear force.

## III. Controller

The controller structure of the proposed mass-spring system representing an aerial manipulator is shown in Fig.4. An output feedback structure is used to design the controller for this project, two states of the four are only needed for the feedback loop in this paper's case; the position and the velocity of the smaller mass (end-effector). A linear quadratic regulator (LQR) will be designed to ensure the stability of the aerial manipulator represented by the mass-spring system, shown in Fig.3, in the presence of wind gusts acting on the manipulator's body (larger mass).

### A. LQR Controller

LQR is a well-known method that provides controlled feedback gains enabling closed-loop stability and high-performance design of systems. Keeping in mind that LQR is a full state feedback, meaning all states are assumed to be measurable. As the main objective of this paper is to exploit the effect of redundancy regarding the end effector's input force, only two states are needed to

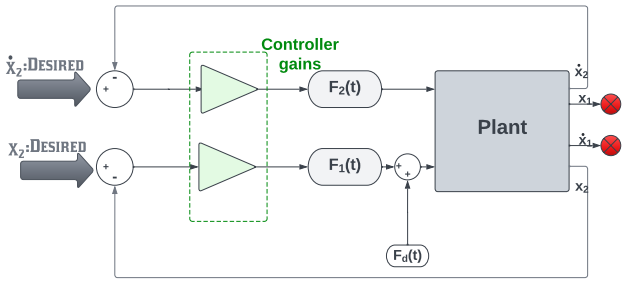


Fig. 4: Control structure of the proposed system in Fig.3

achieve this goal, which is the end effector's position and end effector's velocity. Even though the other two states can be measured and obtained, they will be out of the scope of the controller design. Hence an LQR with output feedback should be designed instead of a full state feedback design. In addition, the output feedback method will allow designing plant controllers for any desired control structure.

The first step is assuming that the plant is given by a linear time-invariant (LTI) state variable model with $x(t) \in R^n$ being the state, $y(t) \in R^p$ the measured output, and $u(t) \in R^m$ the control input.

$$\dot{x} = Ax(t) + Bu(t) \tag{1}$$
$$y(t) = Cx(t) \tag{2}$$

As output feedback is considered, control inputs will be of the form presented in equation (3), where $K$ is an $m \times p$ matrix of constant gains to be determined later by the proposed algorithm.

$$u(t) = -ky(t) \tag{3}$$

The next step is selecting a performance criterion in the time domain to obtain stability of the closed-loop systems, as well as obtaining good time response. The performance index (PI) is going to be considered of type:

$$J = \frac{1}{2}\int_0^\infty x(t)^T Q x(t) + u(t)^T R u(t)\ dt \tag{4}$$

Where $Q$ and $R$ are symmetric positive semidefinite and positive definite weighting matrices, respectively. $Q$ and $R$ definiteness assumptions guarantee a practical minimisation problem since $J$ is always positive. Weighting matrices Q and R can be interpreted as weights, penalising either bad performance or actuator effort, respectively [4]. In general, relative magnitudes of Q and R may be selected to trade off requirements on the smallness of the state against requirements on the smallness of the input

[4]. For instance, a more significant weight of "$Q$" will result in a fast regulation of $x(t)$ to 0 (more aggressive).

The LQR with output feedback goal is the following, given a closed-loop system equation (5) by substituting equations (1) and (3), finding the feedback coefficient matrix $K$ in the control input (3) that minimises the value of the quadratic PI (4).

$$\dot{x} = (A - BKC)x(t) \equiv A_{cl}x(t) \tag{5}$$

The PI can be expressed in terms of K:

$$J = \frac{1}{2}\int_0^\infty (x(t)^T(Q + C^T K^T RKC)x(t))\ dt. \tag{6}$$

The design goal is to select gain $K$ such that $J$ is at the local minimum, subject to the dynamical constraint (5). However, the computational task of finding stabilizing gains becomes a challenge of non-convex numerical optimization, meaning that there is not one minimum value for the cost function $J$. This challenge could be resolved by using the technique of F.L.Lewis et al. [4], which is converting the dynamical optimization into an equivalent static one that is easier to solve. The main idea is to find a constant, symmetric, positive semidefinite matrix $P$ for any fixed feedback matrix $K$ such that it satisfies the Lyapunov equation (7).

$$A_{cl}^T P + PA_{cl} + C^T K^T RKC + Q = 0 \tag{7}$$

Afterwards, if the closed-loop system is stable, then cost $J$ is given in terms of $P$ by equation (8), where $X$ is an $n \times n$ symmetric matrix defined by initial conditions $x(0)x^T(0)$.

$$J = \frac{1}{2}tr(PX),\ \ X = EXP(x_0 x_0^T) \tag{8}$$

### B. Output LQR Design

There are some empirical studies that shows algorithm designs attempts to find LQR gains with output feedback, The problem of designing LQR using output feedback will be addressed in this paper as **OFLQR**. OFLQR is considered to be an NP-hard (non-deterministic polynomial-time hardness) [12] cited in [13], making it one of the most challenging open issues in system science. The main challenges as discussed by Jen-te Yu, [13] are the non-differentiability [6] of the feedback gain and the non-convexity due to product terms of the unknowns in the design equations. As previously discussed, the algorithm used in this project is inspired from Lewis et al. [4] reader. It is a numerical optimization based on the coupled Lyapunov equations (7) & (8), it is generally an iterative algorithm approach presented in table.II:

TABLE II: Optimal Output LQR Feedback Algorithm

1. **Determine an initial gain** $K_0$ **so that** $A - BK_0C$ **is asymptotically stable.**
2. **Solve** $A_{cl}^T P + PA_{cl} + C^T K^T RKC + Q = 0$ **for** $P$ **-Determine** $E\{J\}$ **based on** $J = tr(PX)$
3. **fminsearch(J,K);**

Based on the optimal cost $J$, elements of $K$ would vary to minimise $E\{J\}$ using **Simplex algorithm in Nelder and Mead (1964)**, *fminsearch()*, found in MATLAB (Optimization Toolbox).

There are certain drawbacks to the approach used for solving OFlQR, that needs to be kept in consideration:

- The initial auto correlation of the state is also usually considered to be evenly distributed across the surface of a unit sphere, with $X = I$.
- It is necessary to offer an initial stabilizing output feedback gain, which is not an easy task by its nature as finding a steady output feedback gain has remained a hard, if not equally challenging, task to solve to this day; see Sadabadi and Peaucelle [10] referenced in [13].

## IV. Simulation

Design choices discussed in section II and the underlying assumptions for the controller presented in section III are evaluated and tested in Simulink® software. The goal is to simulate the mass-spring system shown in section II. In particular, we are interested in exploiting the redundancy of the second force applied on the smaller mass while also demonstrating the effects of changing different parameters in the simulation.

In order to simulate the system and investigate the smaller mass position in the presence of wind gusts, one experiment is conducted throughout the whole project, which is inspired by the following video, URL.

The system starts from equilibrium; then, it is disturbed by a pulse, simulating a wind gust of $1N$. Afterwards, it is referenced back to its initial state. This way, we can validate the wind disturbance rejection performance by how much the smaller mass deviates from the equilibrium position.

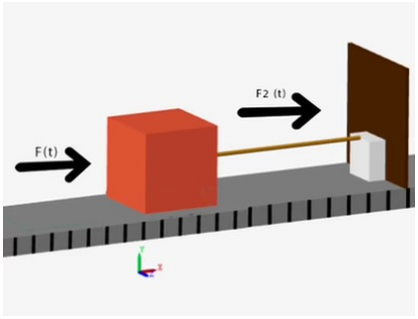


(a) The Redundant Approach

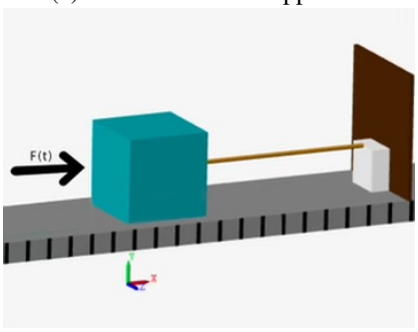


(b) $F(t)$ As The Only Control Input

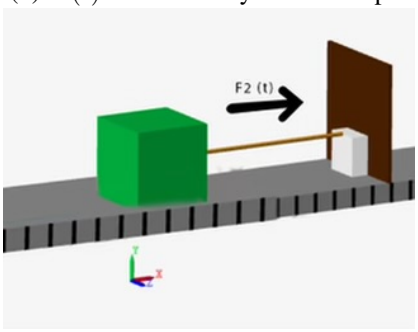


(c) $F_2(t)$ As The Only Control Input

Fig. 5: Setups of the the three conducted approaches in Simulink®: **a)** Two input forces applied on both of the masses $m_2$ (end-effector) & $m_1$ (UAM's body). **b)** Only one force input can be controlled on $m_1$. **c)** Only one force input can be controlled on $m_2$.

## V. Results

In order to present the capabilities and the limitations of the conducted model simulation while exploring the redundancy in the discussed system, experiments were performed (see section IV). Visualizing each experiment is available through this link. In addition more of the resulting figures are shown in appendix A.

Firstly, presenting the results of extensive tests done upon each of the three different cases illustrated in Fig.5, demonstrating the effect of changing the system's physical properties, mainly; the spring stiffness ($K$) and damping coefficient ($b$). Secondly, a comparison between each approach, based upon a specific performance index, which will be discussed after viewing the results for each method.

The wind gust, as mentioned before, is simulated by an exerted step-like force of amplitude $1N$ at the beginning of each experiment. During the experiments, the referenced end-effector's position and velocity are kept constant thought the whole time. Initial model values were chosen as the reference values, which are coloured **blue** in each of the resulting graphs. In the upcoming experiments, each parameter will be decreased and increased relatively to the initial value while keeping other parameters unchanged. In addition, each approach's weighting matrices Q and R (section III) are marked intact. That way we can isolate the effect of each parameter alone. The primary outcomes of each experiment are :

- End-effector's ($m_2$) position.
- UAM body ($m_1$) position.
- Control effort (*Cost*).

These outcomes will be used to assess and derive a pattern for the effect of changing the selected parameters on the system. Even though it is stated that the UAM body position is not referenced to any state, it is still applicable to measure it for observing the overall system behaviour when changing the selected parameters.

### A. *The Redundant Approach*

As illustrated in Table.III, the stiffer the link between both masses ($m_1$) & ($m_2$), the following hold true.

- The maximum position deviation of $m_2$ increases, with the maximum deviation between the lowest and the highest value of $K$ is around 17 $mm$, except for $K = 4Nm^{-1}$ shows a slightly higher peak than at $K = 6Nm^{-1}$
- Almost the same convergence time to the referenced state, with an exception to $K = 8Nm^{-1}$, which shows a faster convergence time.
- For the total work done it seems to decrease except for the $K = 6$, as it result in an abnormal behaviour.

Looking next at increasing the damping coefficient ($b$); no clear conclusion can be drawn as both the higher and the lower value results in a larger position deviation of ($m_2$). This can be explained by the fact that now two control inputs are acting simultaneously, so by tuning the parameters, a random behaviour might occur. Since the cost function is dependent on these changed parameters.

Furthermore, by looking at the maximum position deviation of the bigger mass ($m_1$), we observe that it

moves independently from the smaller mass movement. However, it deviates smaller than the approach with $F_2(t)$ as an only control input. That's because both masses masses are being controlled in this approach.

### B. F(t) As The Only Control Input

As the rod connecting the two bodies (representing the manipulator link) is stiffer, meaning a higher value of $K$ $[Nm^{-1}]$, the following can be deducted from the simulated outcomes presented in Table.IV:

- The maximum position deviation of $m_2$ increases, with the maximum deviation between the lowest and the highest value of $K$ is around $1$ $mm$.
- It is faster to converge to the referenced state, with the maximum time between the lowest and the highest value of $K$ is around 3 seconds.
- The total work done stays almost with no change, but with slight increase.
- The total work done decreases, with the maximum energy difference between the lowest and the highest value of $K$ is around $0.4$ $J$.

The next parameter to asses is the damping coefficient ($b$) as it increases, it is shown to have an inversely proportional relation as opposed to the change in stiffness effect.

- The maximum position deviation of $m_2$ decreases, with the maximum deviation between the lowest and the highest value of $b$ is around $23$ $mm$.
- It is slower to converge to the referenced state, with the maximum time between the lowest and the highest value of $b$ is around 1 second.
- The total work done decreases, with the maximum energy difference between the lowest and the highest value of $b$ is around $0.1$ $J$.

Note that the position behaviour of the bigger mass ($m_1$) is exactly the same as the end-effector position, they tend to move in a rigid-like way.

### C. F2(t) As The Only Control Input

Conclusion about the effect of changing parameters on this approach can be drawn from Table.V. As the link gets stiffer, meaning $K$ has a higher value the following occur:

- The maximum position deviation of $m_2$ increases, with the maximum deviation between the lowest and the highest value of $K$ is around $1.3$ $mm$.
- It is faster to converge to the referenced state, with the maximum time between the lowest and the highest value of $K$ is around 4 seconds.
- The total work done increases, with the maximum energy difference between the lowest and the highest value of $K$ is around $0.1$ $J$.

Jumping to the effect of increasing the damping coefficient ($b$), which has the same effect as on the previous approach.

- The maximum position deviation of $m_2$ decreases, with the maximum deviation between the lowest and the highest value of $b$ is around $1$ $mm$.
- It is slower to converge to the referenced state, with the maximum time between the lowest and the highest value of $b$ is around 7 seconds.
- The total work done decreases, with the maximum energy difference between the lowest and the highest value of $b$ is around $0.2$ $J$.

Note that the maximum position deviation of the bigger mass ($m_1$) is now higher than the smaller mass by almost a factor of 20. That is because there is no any control input applied on the bigger mass in this approach.

### D. What Changes When Redundant Approach is Used

To answer the question of how redundancy affects the system behaviour, a performance criterion has to be set first. Since, the position deviation of the UAM body is out of scope in this research, it will not be considered as one of the performance measures. Therefore, Performance measures is in terms of maximum deviation of the controlled position, convergence time to the referenced state, and the total work done.

First, all three approaches of the same initial parameter values in Table.I were assessed by the accuracy of end-effector ($m_2$) towards the reference state, meaning how much it deviates in respect with the equilibrium position. The redundant approach shows to obtain the best position accuracy of **99.13%** out of all three approaches. Where the other two approaches of $F_2(t)$ or $F(t)$ are the only control inputs have a position accuracy of **98.97%** and **97.38%** respectively. These results can be shown in Fig.6, and can be viewed visually for those interested.

On the other hand, The redundant approach takes a longer time to converge to the referenced $0.6m$ than the $F_2(t)$ as the only control input approach. However, it is still faster to converge to the referenced state than the $F(t)$ as the only control input approach (More details are provided in this link under comparisons folder).

Finally, the steady state total work done by the redundant approach is almost the double of the other two approaches. Keeping in mind that this approach uses two force inputs instead of one.

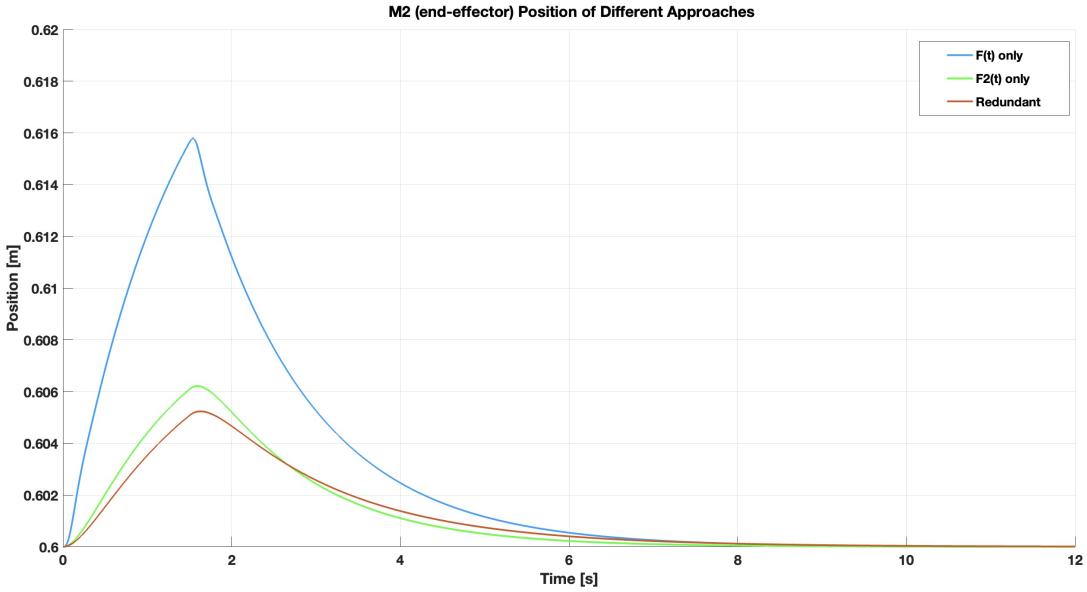


Fig. 6: Comparing $m_2$ position by the three main different approaches

TABLE III: Results of the Redundant Approach

| | | **Different Spring Stiffnesses (K) K [N/m]** | | | | **Different Damping Coefficients (b) b [Ns/m]** | | |
|---|---|---|---|---|---|---|---|---|
| | | K = 4 | ***K = 6*** | K = 8 | K =10 | b = 5 | ***b = 10*** | b = 20 |
| $m_2$ **Position** | **Max. Deviation [mm]** | 5.7 | ***5.2*** | 8.1 | 22.2 | 8.8 | ***5.2*** | 7.9 |
| | **Convergence Time [s]** | 8.5 | ***8.0*** | 5 | 8 | 6.4 | ***8.0*** | 6.7 |
| $m_1$ **Position** | **Max. Deviation [mm]** | 73 | ***63*** | 53 | 47 | 90 | ***63*** | 40 |
| | **Convergence Time [s]** | 16 | ***13*** | 9 | 8 | 8.5 | ***13*** | 15 |
| **Cost** | **Total Work Done [J]** | 3.50 | ***3.56*** | 3.17 | 3.09 | 3.3 | ***3.56*** | 3.2 |

TABLE IV: Results of F(t) as the only control input

| | | **Different Spring Stiffnesses (K) K [N/m]** | | | | **Different Damping Coefficients (b) b [Ns/m]** | | |
|---|---|---|---|---|---|---|---|---|
| | | K = 4 | ***K = 6*** | K = 8 | K =10 | b = 5 | ***b = 10*** | b = 20 |
| $m_2$ **Position** | **Max. Deviation [mm]** | 15.3 | ***15.8*** | 16.1 | 16.4 | 33.0 | ***15.8*** | 10.0 |
| | **Convergence Time [s]** | 9.5 | ***8.5*** | 7 | 6.5 | 8 | ***8.5*** | 9 |
| $m_1$ **Position** | **Max. Deviation [mm]** | 15.2 | ***15.7*** | 16.0 | 16.2 | 32 | ***15.7*** | 8.2 |
| | **Convergence Time [s]** | 10 | ***8*** | 7 | 7 | 7.5 | ***8*** | 9 |
| **Cost** | **Total Work Done [J]** | 1.55 | ***1.55*** | 1.56 | 1.57 | 1.63 | ***1.55*** | 1.52 |

TABLE V: Results of $F_2$(t) as the only control input

| | | **Different Spring Stiffnesses (K) K [N/m]** | | | | **Different Damping Coefficients (b) b [Ns/m]** | | |
|---|---|---|---|---|---|---|---|---|
| | | K = 4 | ***K = 6*** | K = 8 | K =10 | b = 5 | ***b = 10*** | b = 20 |
| $m_2$ **Position** | **Max. Deviation [mm]** | 5.7 | ***6.2*** | 6.6 | 7.0 | 7.1 | ***6.2*** | 5.7 |
| | **Convergence Time [s]** | 11.0 | ***7.6*** | 7.5 | 6.8 | 5.3 | ***7.6*** | 11.8 |
| $m_1$ **Position** | **Max. Deviation [mm]** | 109.0 | ***99.0*** | 90.6 | 83.2 | 142.3 | ***99.0*** | 63.0 |
| | **Convergence Time [s]** | 12.0 | ***9.7*** | 7.4 | 6.2 | 5.0 | ***9.7*** | 14 |
| **Cost** | **Total Work Done [J]** | 1.49 | ***1.52*** | 1.56 | 1.69 | 1.69 | ***1.52*** | 1.49 |

## VI. Conclusion

In this paper, to exploit redundancy in the linearized model of a UAM while regulating its position in the presence of wind gusts, we present extensive tests with an implemented OFLQR algorithm. In particular, we demonstrate how redundancy can help achieve higher accuracy regarding the end-effector's position. However, tests show a tradeoff between the end-effector's position and its convergence time to the reference position. Moreover, we performed numerical simulations of varying parameters to monitor and compare the end-effector's position and the total work done. All Results demonstrate one common aspect: the stiffer the rod, the more the end-effector deviates from the reference state. Hence we show that tuning such property is necessary to provide the desired behaviour. Future work can include a non-linear model instead to get closer to the real-world application. Also, a variational method of OFLQR of Jen-te Yu [13] could be implemented instead of the current one, as it is entirely insensitive to the initial guess of $K_0$. Furthermore, we can consider the m1 position and try limiting the oscillations by implementing an embedded constraint in the controller.

## References


[1] J.T Bartelds, Stefano Stramigioli, and Matteo Fumagalli. "understanding the critical design parameters of aerial manipulators during physical interaction". In: (Aug. 2015).

[2] Chris L. Wilson and Pedro Capo-Lugo. *Robust Control Algorithm for a Two Cart System and an Inverted Pendulum*. Tech. rep. NASA, 2011, pp. 4–5.

[3] Davide Bicego. "Design and Control of Multi-Directional Thrust Multi-Rotor Aerial Vehicles with applications to Aerial Physical Interaction Tasks." PhD thesis. Institut national des sciences appliquées de Toulouse, 2019.

[4] F.L. Lewis. "Applied Optimal Control ". In: *Applied Optimal Control and Estimation: Digital Design and Implementation*. New Jersey: https://lewisgroup.uta.edu, Feb. 1992. Chap. 4, pp. 192–208.

[5] Salua Hamaza, Ioannis Georgilas, and Thomas Richardson. "An adaptive-compliance manipulator for contact-based aerial applications". In: *IEEE/ASME International Conference on Advanced Intelligent Mechatronics, AIM*. Vol. 2018-July. 2018. DOI: 10.1109/AIM.2018.8452382.

[6] Didier Henrion. "Optimization-Based Robust Control". In: *Encyclopedia of Systems and Control*. 2021. DOI: 10.1007/978-3-030-44184-5{_}159.

[7] Franklin E. Pacheco. "An inverted pendulum cart modeled using the bond graph approach". In: *2017 IEEE 2nd Ecuador Technical Chapters Meeting, ETCM 2017*. Vol. 2017-January. 2018. DOI: 10.1109/ETCM.2017.8247507.

[8] Fabio Ruggiero, Vincenzo Lippiello, and Anibal Ollero. "Aerial manipulation: A literature review". In: *IEEE Robotics and Automation Letters* 3.3 (2018). ISSN: 23773766. DOI: 10.1109/LRA.2018.2808541.

[9] Markus Ryll et al. "6D interaction control with aerial robots: The flying end-effector paradigm". In: *International Journal of Robotics Research* 38.9 (2019). ISSN: 17413176. DOI: 10.1177/0278364919856694.

[10] Mahdieh S. Sadabadi and Dimitri Peaucelle. *From static output feedback to structured robust static output feedback: A survey*. 2016. DOI: 10.1016/j.arcontrol.2016.09.014.

[11] Muhammad Shehu et al. "LQR, double-PID and pole placement stabilization and tracking control of single link inverted pendulum". In: *Proceedings - 5th IEEE International Conference on Control System, Computing and Engineering, ICCSCE 2015*. 2016. DOI: 10.1109/ICCSCE.2015.7482187.

[12] Onur Toker and Hitay Ozbay. "On the NP-hardness of solving bilinear matrix inequalities and simultaneous stabilization with static output feedback". In: *Proceedings of the American Control Conference*. Vol. 4. 1995. DOI: 10.1109/acc.1995.532300.

[13] Jen Te Yu. "A Variational Method for Computing Static Output Feedback LQR Gains". In: *7th International Conference on Control, Decision and Information Technologies, CoDIT 2020*. 2020. DOI: 10.1109/CoDIT49905.2020.9263943.

[14] Guangyu Zhang et al. "Aerial grasping of an object in the strong wind: Robust control of an aerial manipulator". In: *Applied Sciences (Switzerland)* 9.11 (2019). ISSN: 20763417. DOI: 10.3390/app9112230.

# 1 $m_2$ Position Deviation With Different Spring Stiffness (K) [N/m]

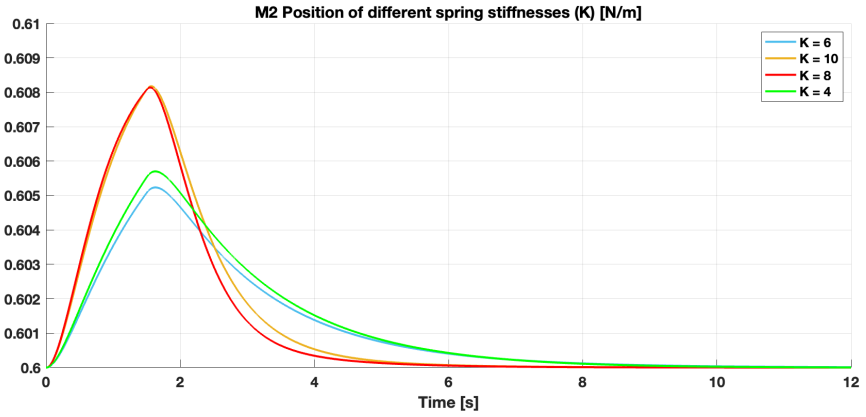


Figure 1: Redundant Approach results

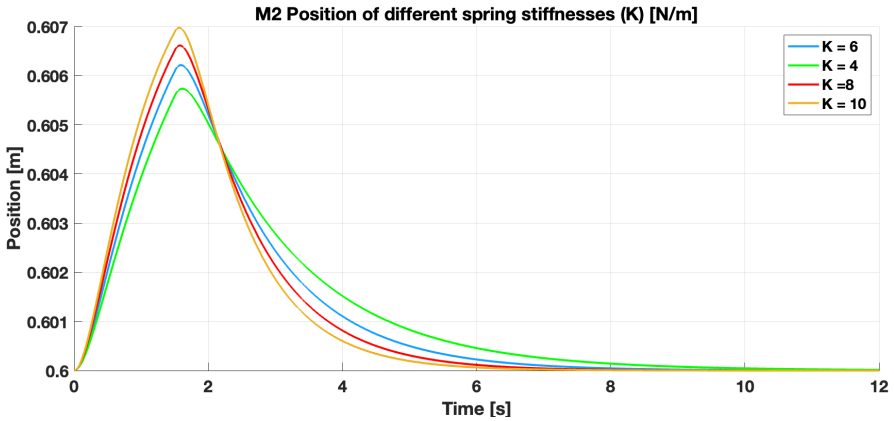


Figure 2: $F_2(t)$ as an only control Input Approach results

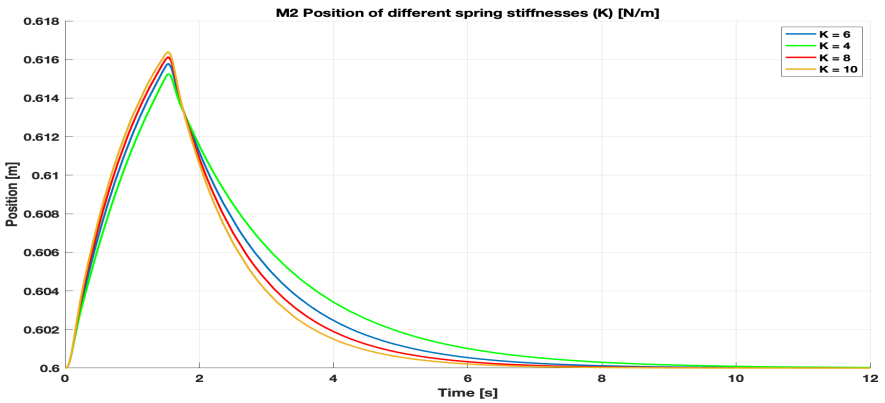


Figure 3: $F(t)$ as an only control Input Approach results

## 2 $m_1$ Position Deviation With Different Spring Stiffness (K) [N/m]

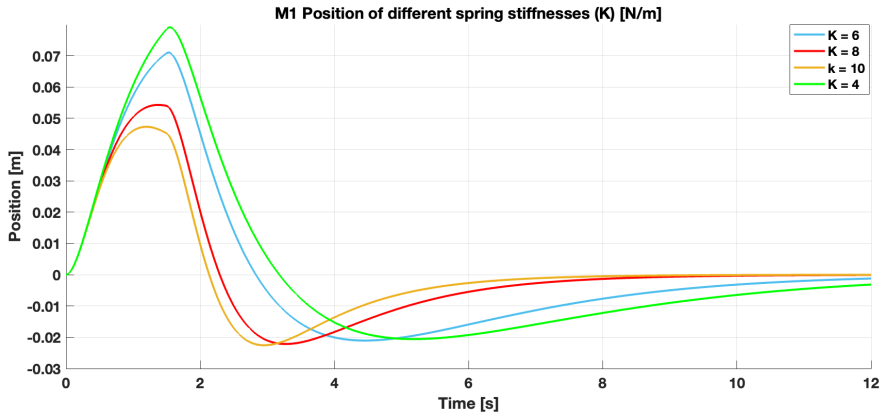


Figure 4: Redundant Approach results

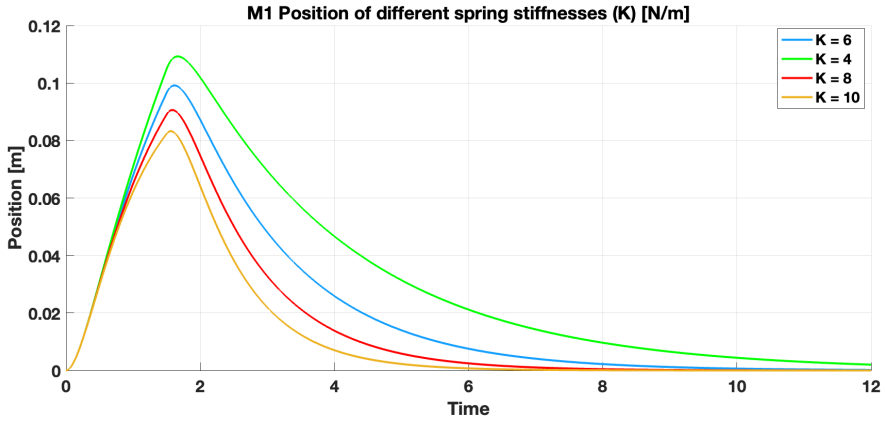


Figure 5: $F_2(t)$ as an only control Input Approach results

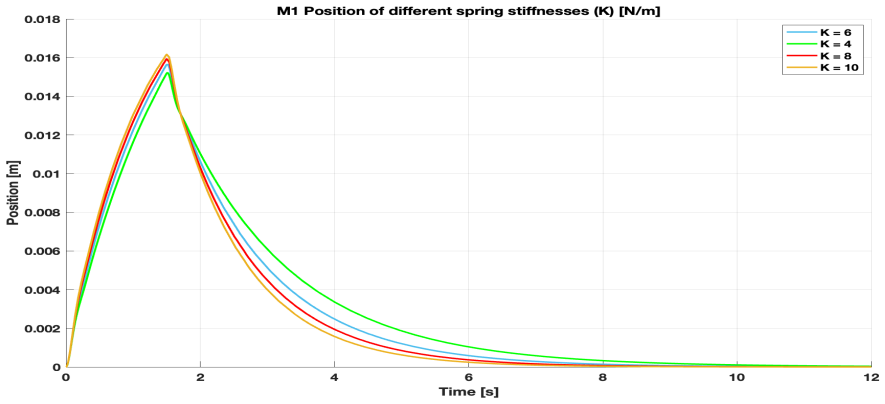


Figure 6: $F(t)$ as an only control Input Approach results

# 3 Work Done by Applying Different Spring Stiffness (K) [N/m]

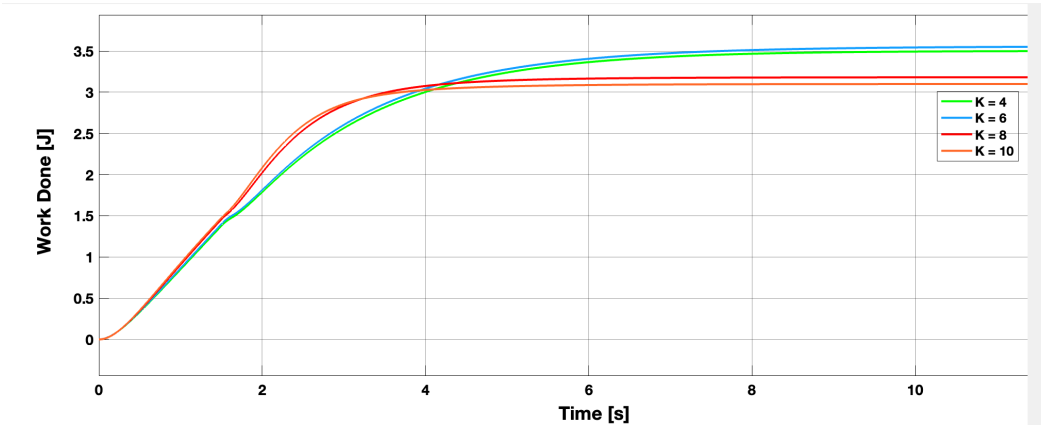


Figure 7: Redundant Approach results

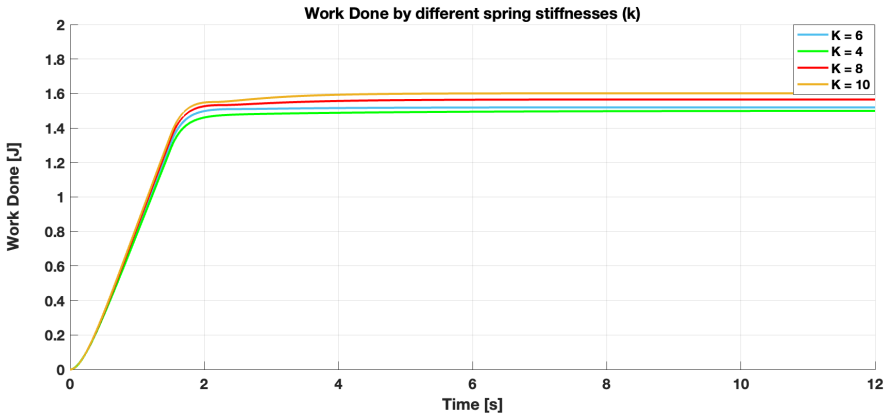


Figure 8: $F_2(t)$ as an only control Input Approach results

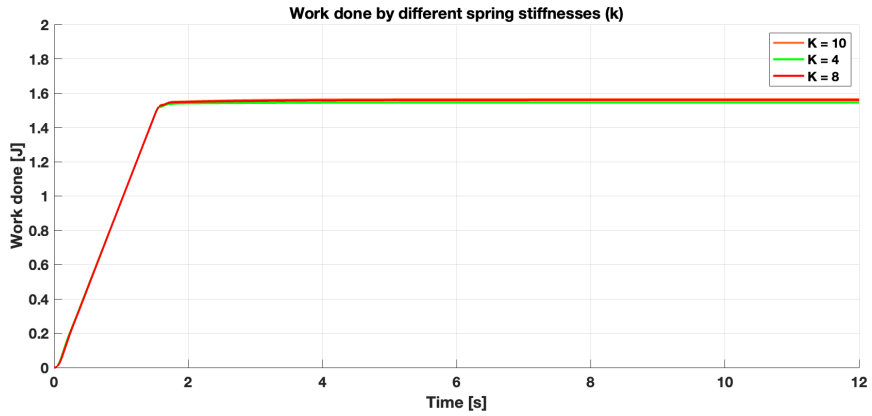


Figure 9: $F(t)$ as an only control Input Approach results

## 4 $m_2$ Position Deviation With Different Damping Coefficient (b)[Ns/m]

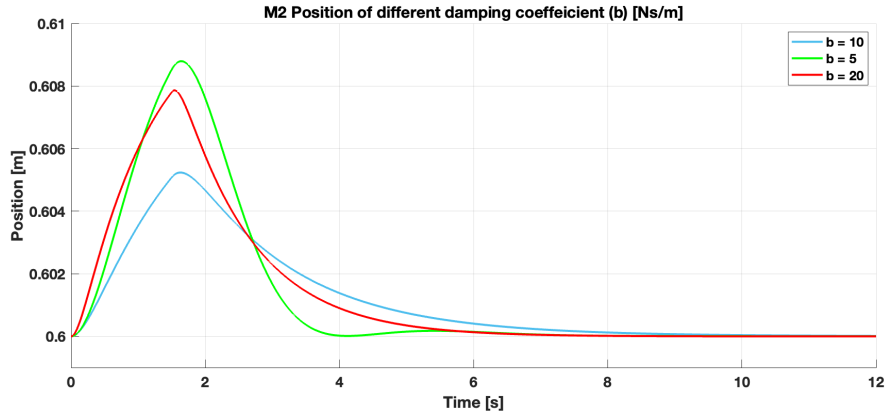


Figure 10: Redundant Approach results

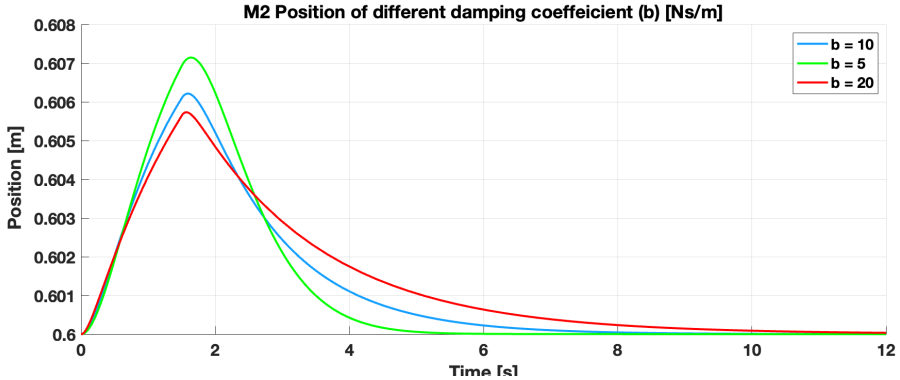


Figure 11: $F_2(t)$ as an only control Input Approach results

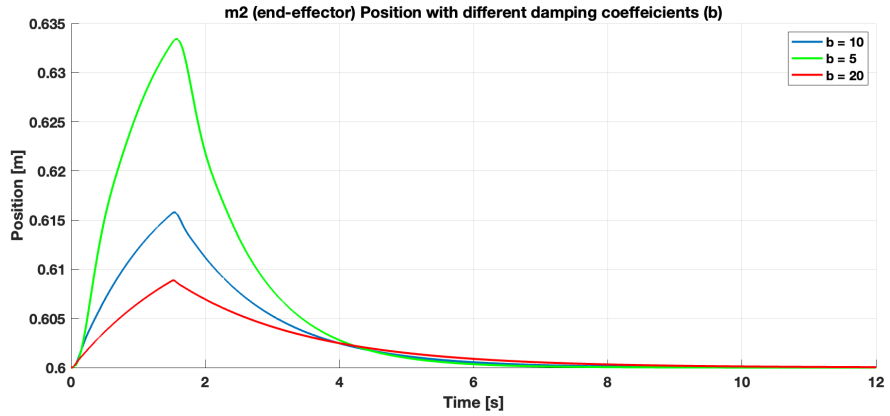


Figure 12: $F(t)$ as an only control Input Approach results

## 5 $m_1$ Position Deviation With Different Damping Coefficient (b)[Ns/m]

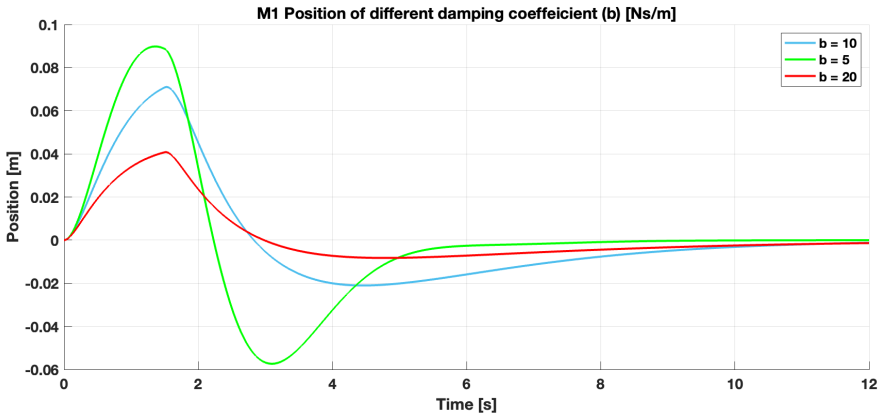


Figure 13: Redundant Approach results

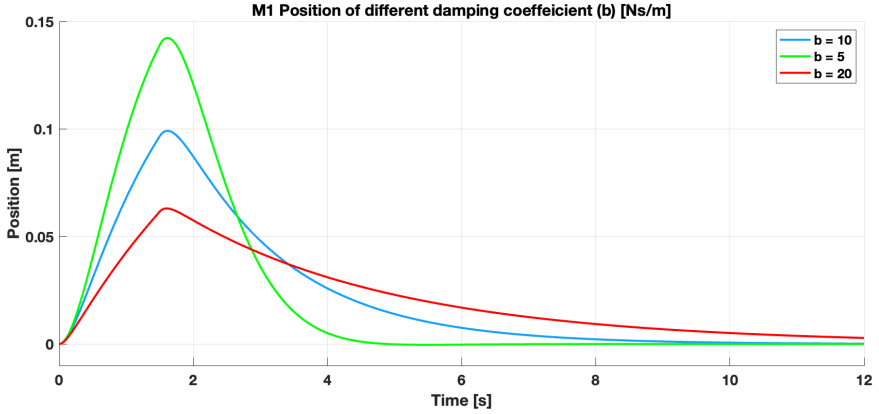


Figure 14: $F_2(t)$ as an only control Input Approach results

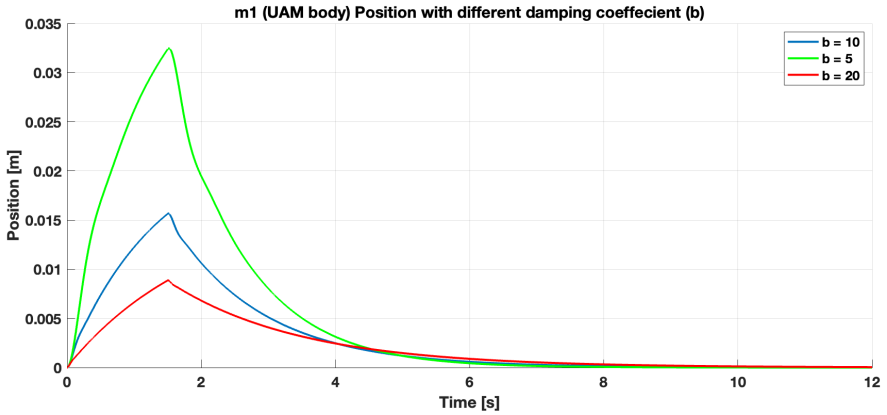


Figure 15: $F(t)$ as an only control Input Approach results

# 6 Work Done by Applying Different Damping Coefficient (b)[Ns/m]

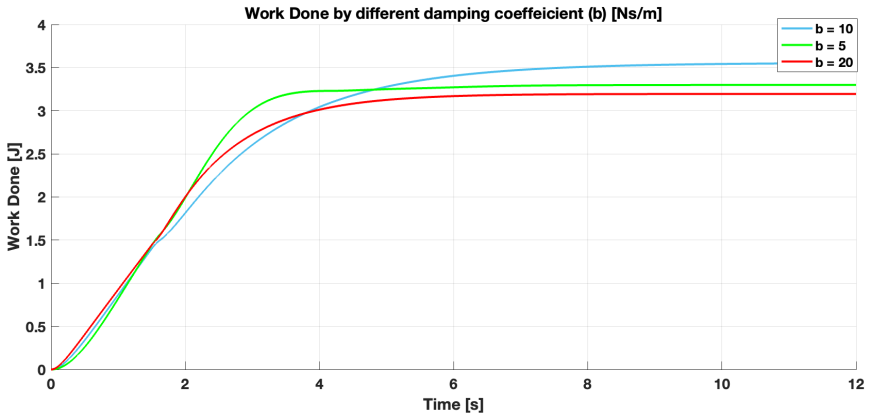


Figure 16: Redundant Approach results

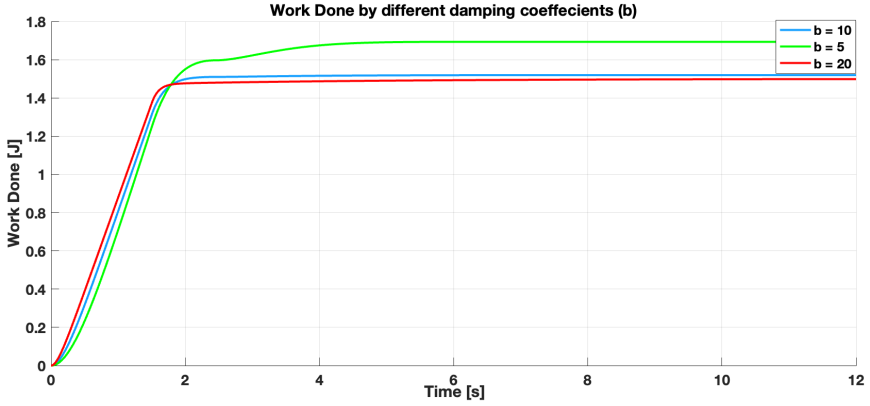


Figure 17: $F_2(t)$ as an only control Input Approach results

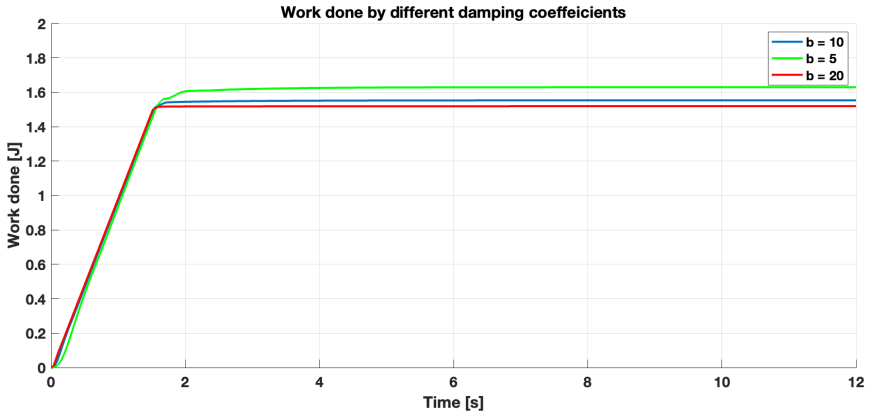


Figure 18: $F(t)$ as an only control Input Approach results